Since January 2020 Elsevier has created a COVID-19 resource centre with free information in English and Mandarin on the novel coronavirus COVID-19. The COVID-19 resource centre is hosted on Elsevier Connect, the company's public news and information website.

Journal Pre-proof

Inosine: a broad-spectrum anti-inflammatory against SARS-CoV-2 infection-induced acute lung injury via suppressing TBK1 phosphorylation

Ningning Wang, Entao Li, Huifang Deng, Lanxin Yue, Lei Zhou, Rina Su, Baokun He, Chengcai Lai, Gaofu Li, Yuwei Gao, Wei Zhou, Yue Gao

PII: S2095-1779(22)00098-3

DOI: https://doi.org/10.1016/j.jpha.2022.10.002

Reference: JPHA 741

To appear in: *Journal of Pharmaceutical Analysis*

Received Date: 28 June 2022

Revised Date: 14 October 2022

Accepted Date: 17 October 2022

Please cite this article as: N. Wang, E. Li, H. Deng, L. Yue, L. Zhou, R. Su, B. He, C. Lai, G. Li, Y. Gao, W. Zhou, Y. Gao, Inosine: a broad-spectrum anti-inflammatory against SARS-CoV-2 infection-induced acute lung injury via suppressing TBK1 phosphorylation, *Journal of Pharmaceutical Analysis*, https://doi.org/10.1016/j.jpha.2022.10.002.

Inosine: a broad-spectrum anti-inflammatory against SARS-CoV-2 infection-induced acute lung injury via suppressing TBK1 phosphorylation

Ningning Wang [a, b, 1], Entao Li [c, 1], Huifang Deng [a, 1], Lanxin Yue [a], Lei Zhou [a], Rina Su [c, d], Baokun He [e], Chengcai Lai [a], Gaofu Li [a], Yuwei Gao [c, *], Wei Zhou [a, **], Yue Gao [a, b, ***]

[a] *Department of Pharmaceutical Sciences, Beijing Institute of Radiation Medicine, Beijing, 100850, China.*

[b] *Tianjin University of Traditional Chinese Medicine, Tianjin, 301617, China.*

[c] *Changchun Veterinary Research Institute, Chinese Academy of Agricultural Sciences, Changchun, 130122, China.*

[d] *College of Veterinary Medicine, Jilin Agricultural University, Jilin, 130022, China.*

[e] *Department of Gastroenterology, Shanghai General Hospital, Shanghai Jiao Tong University School of Medicine, Shanghai 200080, China.*

[1] These authors contributed equally to this work.

---

[*]Corresponding author: Yuwei Gao, E-mail: yuwei0901@outlook.com, Changchun Veterinary Research Institute, Chinese Academy of Agricultural Sciences,Changchun, 130122, China.

[**]Corresponding author: Wei Zhou, E-mail: zhouweisyl802@163.com, Department of Pharmaceutical Sciences, Beijing Institute of Radiation Medicine, Beijing, 100850, China.

[***]Corresponding author: Yue Gao, E-mail: gaoyue@bmi.ac.cn, Department of Pharmaceutical Sciences, Beijing Institute of Radiation Medicine, Beijing, 100850, China.

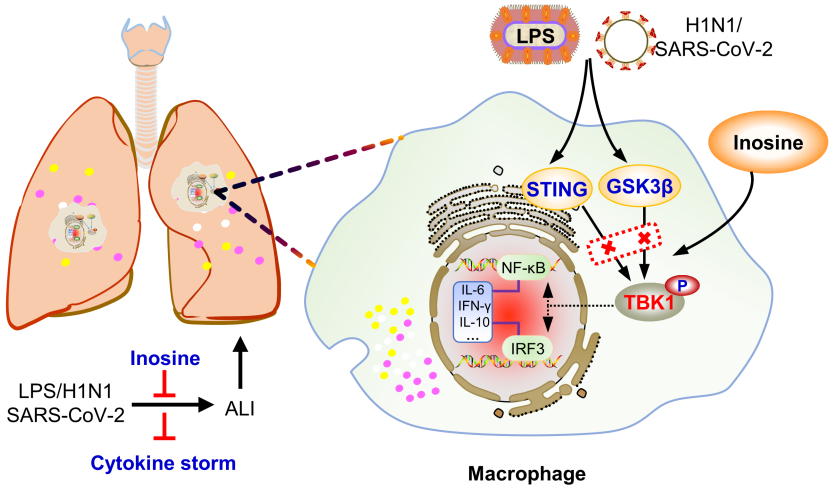

Inosine: a broad-spectrum anti-inflammatory against SARS-CoV-2 infection-induced acute lung injury via suppressing TBK1 phosphorylation

Abstract

SARS-CoV-2-induced cytokine storms constitute the primary cause of COVID-19 progression, severity, criticality, and death. Glucocorticoid and anti-cytokine therapies have been frequently administered to treat COVID-19 but have had limited clinical efficacy in severe and critical cases. Nevertheless, the weaknesses of these treatment modalities have prompted the development of anti-inflammatory therapy against this infection. We found that the broad-spectrum anti-inflammatory agent inosine downregulated proinflammatory IL-6, upregulated anti-inflammatory IL-10, and ameliorated acute inflammatory lung injury caused by multiple infectious agents. Inosine significantly improved survival in mice infected with SARS-CoV-2. It indirectly impeded TANK-binding kinase 1 (TBK1) phosphorylation by binding stimulator of interferon genes (STING) and glycogen synthase kinase-3β (GSK3β), inhibited the activation and nuclear translocation of the downstream transcription factors IRF3 and NF-κB, and downregulated IL-6 in the sera and lung tissues of mice infected with lipopolysaccharide (LPS), H1N1, or SARS-CoV-2. Thus, inosine administration is feasible for clinical anti-inflammatory therapy against severe and critical COVID-19. Moreover, targeting TBK1 is a promising strategy for inhibiting cytokine storms and mitigating acute inflammatory lung injury induced by SARS-CoV-2 and other infectious agents.

22 **Keywords:** Cytokine storm, Interleukin 6, Inosine, SARS-CoV-2, TANK-binding

23 kinase 1 (TBK1)

24

1. Introduction

The coronavirus disease 19 (COVID-19) pandemic is caused by severe acute respiratory syndrome coronavirus 2 (SARS-CoV-2) infection and has rapidly led to a global health crisis [1]. By the end of 2021, over 250 million people worldwide were diagnosed with COVID-19. Ten to fifteen percent of these cases progressed to severe or critical status and over five million people died [2, 3]. Newly developed antiviral drugs have demonstrated a certain degree of efficacy against mild COVID-19 [4]. Cases that progressed to severe or critical status were characterized by a pulmonary hyperinflammatory state known as a cytokine storm [5]. In these cases, only anti-inflammatory therapy is potentially clinically beneficial [6]. Though immunosuppressive glucocorticoids reduced the requirement for mechanical ventilation, they did not significantly lower mortality in severe and critical cases [7, 8]. In fact, they sometimes worsened the condition by delaying viral clearance [9]. The ideal therapeutic agent for severe or critical COVID-19 controls cytokine release and prevents overactivation of the immune response.

Cytokine storms cause life-threatening systemic inflammation characterized by immune cell hyperactivation and the release of proinflammatory cytokines including interleukin-6 (IL-6), interferons, and tumor necrosis factor-alpha (TNF-α) [10]. Our previous study and several recent articles indicated that a sharp increase in pleiotropic cytokine IL-6 content was associated with acute respiratory distress syndrome (ARDS), sepsis, and even death in patients with COVID-19 [11, 12]. IL-6 receptor antagonists have been widely administered in human clinical trials. However, IL-6 signaling

blockade provided no broad-based survival benefit in COVID-19 therapy. A possible explanation is that IL-6 is essential for activating innate/adaptive immunity and facilitating efficient pathogen clearance [13, 14]. Therefore, it is necessary to develop a transcriptional regulation strategy wherein the SARS-CoV-2-induced rise in IL-6 content is controlled and the anti-inflammatory response initiated by IL-6 is partially conserved.

Viral genes are detected by classical Toll-like receptors (TLRs) as well as other specific pattern recognition receptors (PRRs) that initiate the host innate immune response. Viral RNA is detected by retinoic acid-inducible gene I (RIG-I)-like receptors (RLRs) while viral DNA is sensed by cyclic GMP-AMP synthase (cGAS) [15]. In turn, RIG-I and cGAS activate particular signaling cascades and induce IL-6 and other inflammatory cytokines via mitochondrial antiviral signaling (MAVS) protein and stimulator of interferon genes (STING), respectively [16, 17]. The RNA virus SARS-CoV-2 can evade RLR sensors and inhibit the MAVS downstream adaptor [18]. By contrast, host self-DNA in the cytoplasms of SARS-CoV-2-induced syncytia triggers the antiviral innate immune response via the cGAS-STING pathway [15], activates interferon regulatory factor (IRF3) and nuclear factor kappa B (NF-κB), induces interferons, and upregulates proinflammatory cytokines [19]. Glycogen synthase kinase-3-beta (GSK3β) is activated in SARS-CoV-2-infected cells and is required for viral replication [20]. Activated GSK3β phosphorylates NF-κB and provokes systemic inflammation [21]. Hence, multiple signaling pathway-induced NF-κB responses may control IL-6 transcription and release in patients with COVID-19. Recent evidence

demonstrated that TANK-binding kinase 1 (TBK1) is a vital factor in the foregoing innate immune signaling pathways and mediates upstream stimuli and downstream NF-κB or IRF3 signaling [22]. For these reasons, suppressing TBK1 activation could modulate the host innate immune response following SARS-CoV-2 infection.

Inosine is a type of purine nucleoside. It is a deamination metabolite of adenosine and is also formed by binding hypoxanthine with ribose. Endogenous inosine is a key intermediate in purine biosynthesis and regulates RNA replication and translation [23]. Exogenous inosine supplementation protects against lipopolysaccharide (LPS)-induced acute lung injury and endotoxin-induced septic shock by suppressing the release of the proinflammatory cytokines IL-6, IL-1β, TNF-α, and so on [24, 25]. Inosine may also modulate Th1 cell differentiation and/or activation and improve immunotherapy efficacy via the T cell-specific adenosine A_{2A} receptor ($A_{2A}R$) and STING signaling pathways [26, 27]. Inosine was detected in certain Chinese material medica and medical formulae such as *Lumbricus terrestris* and *Pinellia ternata* (Thunb.) that are administered for the treatment of pneumonia and COVID-19 [28, 29]. Hence, inosine might control SARS-CoV-2-induced cytokine storms.

Here, we found that inosine functioned as a broad-spectrum anti-inflammatory agent. It attenuated acute lung inflammatory injury triggered by various stimuli and markedly improved survival in mice infected with SARS-CoV-2. Inosine demonstrated strong efficacy against cytokine storms as it inhibited innate immune signaling-mediated TBK1 phosphorylation by multiple routes. The findings of this work showed that inosine could serve as an adjuvant for the treatment of severe or critical COVID-

19 and suggested that TBK1 is a potential therapeutic target.

2. Materials and Methods

2.1 Cell lines and viruses

All cell lines used in the present study were purchased from the National Infrastructure of Cell Line Resource (Beijing, China). Mouse leukemic monocyte/macrophages (RAW264.7) and human embryonic kidney 293 (HEK293) cells were maintained in a humidified incubator (37 °C, 5% CO_2) in Dulbecco's modified Eagle's medium (DMEM) (Thermo Fisher Scientific Inc., Waltham, MA, USA) containing 10% (*V/V*) fetal bovine serum (FBS, Tianhang Biotechnology, Hangzhou, China) and antibiotics (100 U/mL penicillin and 100 mg/mL streptomycin) (Sigma-Aldrich Corp., St. Louis, MO, USA). Influenza A (H1N1) virus Beijing/501/2009 strain (BJ501) was isolated from a patient in Beijing confirmed to be infected in 2009. The genome sequence of this strain appears in the GenBank database (https://www.ncbi.nlm.nih.gov/genbank/) under accession No. GQ223415. The mouse-adapted SARS-CoV-2 C57MA14 strain was isolated from a COVID-19 patient in Wuhan, China and obtained by continuous passage in C57BL/6N mice. The genome sequence of this strain appears in the GenBank database under accession No. OL913104.1. All experiments involving live H1N1 virus and SARS-CoV-2 were performed in a biosafety level three (BSL-3) laboratory at the Changchun Veterinary Research Institute of the Chinese Academy of Agricultural Sciences and in strict accordance with biosafety standard operating procedures.

2.2 Reagents and methods

Lipopolysaccharide (LPS; purity ≥ 98%) and dexamethasone sodium phosphate (DXM; purity ≥ 99%) were obtained from Solarbio Science & Technology (Beijing, China). Poly(I:C) (purity ≥ 99%) was purchased from Sigma-Aldrich Corp. (St. Louis, MO, USA). High-quality specific agonists or antagonists of STING, TBK1, GSK3β, and $A_{2A}R$ were purchased from Topscience Co., Ltd. (Shanghai, China). Primary anti-$A_{2A}R$ antibody was obtained from Proteintech Co., Ltd. (Wuhan, China). Anti-phospho-GSK3β (p-GSK3β), anti-GSK3β, anti-phospho-STING (p-STING), anti-STING, anti-phospho-TBK1 (p-TBK1), anti-TBK1, anti-phospho-IRF3 (p-IRF3), anti-IRF3, anti-phospho-NF-κB (p-NF-κB), anti-NF-κB, anti-IL-6, anti-GAPDH, and anti-rabbit immunoglobulin G (IgG) horseradish peroxidase (HRP)-conjugated secondary antibodies were purchased from Cell Signaling Technology, Inc. (Danvers, MA, USA).

2.3 Biosafety facility and ethics statement

All work involving live SARS-CoV-2 viruses was conducted in a BSL-3 laboratory at the Changchun Veterinary Research Institute of the Chinese Academy of Agricultural Sciences. The BALB/c mice were housed and maintained in accordance with the Guidelines for the Welfare and Ethics of Laboratory Animals of China. All animal studies were approved by the Animal Welfare and Ethics Committee of the Changchun Veterinary Research Institute of the Chinese Academy of Agricultural Sciences under approval No. IACUC-AMMS-11-2020-020.

2.4 Mouse husbandry and treatment

C57BL/6N mice aged 7−10 weeks and weighing 20−22 g and BALB/c mice aged 9 months and weighing 25−30 g were obtained from the Beijing Charles River

Laboratory Animal Co., Ltd. (Beijing, China). The mice were maintained under specific pathogen-free (SPF) conditions and ~12 h light:12 h dark cycles. The SARS-CoV-2 challenge was performed on BALB/c mice. They were intranasally infected with 50 μL of a 10^3 median tissue culture infective dose ($TCID_{50}$) SARS-CoV-2 strain C57MA14. The C57BL/6N mice were exposed to H1N1 virus or LPS by intranasal inoculation or intratracheal instillation, respectively. Mice exposed to SARS-CoV-2, H1N1 virus, or LPS were randomly assigned either to an inosine treatment group or a vehicle group. The animals in the control group were administered equivalent volumes of sterile saline solution by intranasal inoculation or intratracheal instillation. Mouse survival and body weight changes were monitored daily. All experimental protocols were approved by the Ethics Committee of Animal Experiments of the Beijing Institute of Radiation Medicine under approval No. IACUC-DWZX-2020-762.

2.5 Viral RNA extraction and RT-qPCR

The mouse tissues were mixed with DMEM and homogenized (homogenizer, Thermo Fisher Scientific Inc.) for 5 min. The suspension was centrifuged at 12,000 *g* and 4 ℃ for 10 min and the supernatant was conserved. The RNA viruses were extracted with a QIAamp Viral RNA Mini Kit (QIAGEN, Dusseldorf, Germany). The viral RNA was quantified by RT-qPCR with Premix Ex Taq (Takara, Beijing, China) targeting the SARS-CoV-2 *N* gene. The primer and probe sequences were as follows: NF (5′-GGGGAACTTCTCCTGCTAGAAT-3′); NR (5′-CAGACATTTTGCTCTCAAGCTG-3′); and NP (5′-FAM-TTGCTGCTGCTTGACAGATT-TAMRA-3′).

157 *2.6 SARS-CoV-2 load quantification by $TCID_{50}$*

158 The supernatants of the lung and turbinate bone tissue homogenates were diluted
159 with DMEM and applied to Vero E6 cells cultured on 96-well plates (Corning Inc.,
160 Corning, NY, USA). The Vero E6 cells were incubated for 1 h and the DMEM was
161 replenished. After 72 h incubation, the $TCID_{50}$ was determined based on the cytopathic
162 effect.

163 *2.7 Serum cytokine/chemokine measurements*

164 Mice were euthanized at 1 day or 3 day post-infection/treatment and their sera
165 were collected. Serum cytokines were measured with a ProcartaPlex Mouse Cytokine
166 Panel (Thermo Fisher Scientific Inc.). The assays were conducted in 96-well filter
167 plates and in a flow-based instrument (Luminex® 200™; Thermo Fisher Scientific Inc.)
168 according to the manufacturer's instructions. Serum IL-6 levels were confirmed with a
169 Sandwich enzyme-linked immunosorbent assay (ELISA) kit (Meimian industrial Co.,
170 Ltd, Yancheng, China). All data were calculated by deducting the background value.

171 *2.8 Histological analysis and immunofluorescence*

172 Mice were sacrificed at 1 day or 3 day post-infection/treatment and their lungs
173 were harvested and fixed in 10% (*V/V*) neutral buffered formalin, embedded in paraffin,
174 cut into 3.5-μm sections (Leica, Weztlar, Germany), and subjected to hematoxylin-
175 eosin (H&E) staining. For the lung tissue immunofluorescence assay, the sections were
176 sealed with bovine serum albumin (BSA) at 25 °C for 30 min and incubated at 4 °C
177 overnight with the indicated primary antibodies. The slides were then incubated with
178 fluorescein isothiocyanate (FITC) anti-rabbit secondary antibody and 4`,6-diamidino-

2-phenylindole (DAPI) containing anti-fluorescence quenching agent. The lung sections were then visualized under a whole-slide imaging microscope fitted with Pannoramic Scanner software (Pannoramic DESK, Budapest, Hungary). RAW264.7 cells were fixed with immunostaining fixing solution (Beyotime Biotechnology, Shanghai, China) and blocked with immunostaining blocking buffer (Beyotime Biotechnology). The corresponding primary antibody was incubated at 4 °C overnight. The cells were then washed with phosphate-buffered saline (PBS) and incubated with fluorescently-coupled secondary antibodies and DAPI. Fluorescence images were visualized under a confocal laser scanning microscope (CLSM; Carl Zeiss AG, Oberkochen, Germany).

2.9 Western blot

Proteins were extracted from the cells or lung tissue with cold radioimmunoprecipitation assay (RIPA) buffer and quantified by bicinchoninic acid (BCA) assay. The proteins were separated on 10% sodium dodecyl sulfate (SDS)-polyacrylamide gels (Epizyme Biomedical Technology Co., Ltd, Shanghai, China) and transferred onto polyvinylidene fluoride (PVDF) membranes (EMD Millipore, Billerica, MA, USA). The latter were sealed with 5% skim milk and successively incubated with the indicated primary and secondary antibodies. The bands were incubated with SuperSignal West Pico PLUS Detection Reagent (Thermo Fisher Scientific Inc.) and visualized with ImageQuant LAS 500 (GE Healthcare BioSciences AB, Chicago, IL, USA).

2.10 Co-immunoprecipitation (Co-IP) assay

The TBK1 cDNA sequence was cloned into a pCDNA3.1 expression plasmid and fused with HA-tag at the *C*-terminal. HEK293 cells were transfected with 2 μg TBK1-HA expression plasmid using Lipofectamine™ 2000 (Invitrogen, Carlsbad, CA, USA) according to the manufacturer's instructions. The cells were collected and resuspended in lysis buffer containing protease and phosphatase inhibitors. The lysates were mixed with rabbit monoclonal anti-HA at 4 °C overnight to form the immune complex. Prewashed Pierce™ classic magnetic beads (Thermo Fisher Scientific Inc.) were added to the lysate samples and the mixture was incubated at room temperature for 1 h. The beads were harvested on a magnetic rack, washed thrice with cold rinse buffer, and eluted with eluent. The proteins were eluted from the beads by boiling with loading buffers and then subjected to immunoblot analysis.

2.11 Biotin-tagged inosine synthesis

To identify binding between inosine and its targets, the former was labeled with biotin at its hydroxyl moiety and biotinylated inosine (Bio-inosine) was synthesized. One equivalent biotin was dissolved in dry dimethyl sulfoxide (DMSO), 1.2 eq *N*,*N*,*N*`,*N*`-tetramethyl-*O*-(*N*-succinimidyl)uronium tetrafluoroborate (TSTU) and 0.1 mL triethylamine were added, and the reaction was conducted at room temperature for 4 h. Then diethyl ether was added to precipitate the biotin succinimidyl ester (SE). Then 1 eq biotin SE was dissolved in 2 mL *N*,*N*-dimethylformamide (DMF) and dripped into DMF containing 1 eq inosine through a constant-pressure dropping funnel for 4 h. The reaction continued for another 4 h and the solvent was evaporated at low pressure to prepare the liquid phase for purification. Bio-inosine structure and purity were

223 determined by nuclear magnetic resonance (Bruker AVANCE NEO, karlsruhe,
224 Germany) and liquid chromatography-mass spectrometry-ion trap-time-of-flight
225 (LC/MS-IT/TOF; Shimadzu, Japan) (Figs. S4A and S4B). The inosine successfully
226 bound the biotin and the target compound was relatively pure.

227 *2.12 Biotin pulldown assay*

228 Streptavidin isolated from *Streptomyces avidinii* was covalently bound to agarose
229 to perform pull-down experiments. Five hundred microliters of 500 μM Bio-inosine or
230 biotin was added to 60 μL streptavidin-agarose beads (Sigma-Aldrich Corp.) and
231 incubated at 4 °C overnight. The cell lysates were then added to the streptavidin-agarose
232 beads containing Bio-inosine or biotin. The mixture was placed in a blender, incubated
233 at 4 ℃ overnight, and washed thrice with PBS. The bead-bound proteins were boiled
234 in 2× loading buffer and subjected to immunoblot analysis on SDS-polyacrylamide gels.

235 *2.13 Computational docking and molecular simulation*

236 Docking was performed using the Glide module in Schrödinger 2020-2 software
237 (https://www.schrodinger.com/releases/release-2020-2). The protein structures used in
238 the docking studies included human GSK3β and STING. Their pdb codes were 1Q5K
239 and 6UKZ, respectively. All crystal structures were prepared according to the
240 recommended procedure in the Protein Preparation Wizard
241 (https://www.schrodinger.com/science-articles/protein-preparation-wizard). The
242 ligands and solvent molecules were removed. Polar hydrogen atoms were added for
243 each protein structure and the atomic charges were assigned based on the OPLS3e force
244 field. Residues within 20 Å of the active ligand binding sites in the crystal structure

were defined as the binding sites at which the docking grids were created. The ligand structures were prepared with the LigPrep module (https://www.schrodinger.com/products/ligprep) to define the protonation state and the atomic charges (reference pH = 7.0 ± 2.0; OPLS3e force field). The native ligand was removed and docking was conducted in standard docking mode with the receptor. The default input parameters were (a) no scaling factor for the VdW radii of the nonpolar protein atoms, and (b) 0.8 scaling factor for the nonpolar ligand atoms. Both were used in all computations. Inosine was docked and scored in Glide standard precision (SP) mode and the optimal inosine pose was selected with Glide Score. The binding interaction modes of inosine with human GSK3β and STING were analyzed with PyMOL (https://pymol.org/2/).

2.14 Statistical analysis

Statistical analyses were conducted in GraphPad Prism 8.0 (GraphPad Software, La Jolla, CA, USA). The data were means ±standard error of the mean (SEM). One-way analysis of variance (ANOVA) followed by a least significant difference (LSD) post-hoc test compared multiple treatment means. A log-rank (Mantel-Cox) test was used to determine mouse survival rates. $P < 0.05$ indicated statistical significance.

3. Results

3.1 Inosine alleviated LPS- and H1N1 virus-induced acute inflammatory lung injury by regulating cytokine secretion

We used LPS and H1N1 virus to establish acute inflammatory lung injury models in mice and evaluate the anti-inflammatory effect of inosine. H&E staining revealed

obvious inflammatory cell infiltration and patchy hemorrhage in the alveolar cavity and the pulmonary interstitium at 24 h post LPS treatment (Fig. 1A). These signs were accompanied by sharp increases in serum IL-6 and IFN-γ levels and remarkable changes in bodyweight and wet-to-dry lung weight ratio (W/D) (Figs. 1B, S1A and S1B). Elevated IL-6 was detected in both the LPS-infected lung tissue and the RAW246.7 cells (Figs. 1C and D). Both DXM and the 300 mg/kg inosine treatment inhibited LPS-induced increases in serum IL-6 and IFN-γ (Fig. 1B), lowered the IL-6 content in LPS-infected mouse lung tissue (Fig. 1C) and mononuclear macrophages (Fig. 1D), and ameliorated LPS-induced lung tissue damage (Fig. 1A). Inosine significantly upregulated serum IL-10 content in the mouse model (Fig. 1B). The 900 mg/kg inosine treatment attenuated H1N1-induced serum IL-6 upregulation and acute lung injury in mice within the first 24 h post-infection (Figs. 1E and F). Inosine had a weaker antagonistic effect than DXM against H1N1-induced histopathology but exerted no adverse effect on mouse body weight (Fig. S1C). The preceding results suggest that inosine has broad-spectrum anti-inflammatory efficacy in COVID-19 therapy by controlling the cytokine storm.

3.2 Inosine improved survival in SARS-CoV-2-infected mice by alleviating inflammatory injury rather than through antiviral activity

We performed in vivo antiviral assays to determine whether inosine alleviates SARS-CoV-2-induced acute lung injury. The mice were orally administered single daily inosine doses at 24 h before C57MA14 infection and were sacrificed at 1 day, 3 day or 14 day post infection (dpi) (Fig. 2A). Inosine did not lower SARS-CoV-2 copies

and titers in infected mouse lung and nasal turbinate tissues at 1 dpi and at 3 dpi (Fig. 2B and Fig. S2A). However, inosine treatment substantially lowered serum IL-6 and IFN-γ and raised serum IL-10 and IL-22 at 1 dpi or 3 dpi (Fig. 2C and Fig. S2B). Inosine ameliorated the pathological changes in the lungs and maintained normal pulmonary structure at the early stages of infection (Fig. 2D). After 14 day, all the mice in the SARS-CoV-2 group had died (Fig. 2E). However, daily oral inosine administration impeded weight loss starting at 9 dpi (Fig. 2F) and dramatically improved survival in mice infected with SARS-CoV-2 (Fig. 2E). Inosine also prevented SARS-CoV-2 infection from inducing inflammatory lesions in the lungs of the mice still surviving at 14 dpi (Fig. S2C). Inosine also inhibited pulmonary IL-6 and mononuclear macrophage activation induced by SARS-CoV-2 infection (Figs. 2G and H). Hence, inosine might have improved survival in SARS-CoV-2-infected mice by regulating cytokine release.

3.3 STING and GSK3β signaling participated in the acute inflammatory response induced by various infectious agents

We then sought to identify the innate immune signaling involved in the acute inflammatory response induced various infectious agents. The in vitro experiments showed that LPS and SARS-CoV-2 activated cGAS-STING and GSK3β signaling. Both infectious agents increased STING and GSK3β phosphorylation at Ser365 and Ser9, respectively (Fig. 3A). By contrast, Poly(I:C) only induced GSK3β phosphorylation and had no apparent influence on the cGAS-STING pathway (Fig. 3A). LPS, Poly(I:C), and SARS-CoV-2 activated the proinflammatory nuclear factors NF-κB and IRF3 (Fig. 3A). STING inhibitor (H151) or GSK3β inhibitor (TWS119) co-

311 administration noticeably reduced NF-κB and IRF3 phosphorylation in RAW246.7
312 cells infected with LPS, Poly(I:C), or SARS-CoV-2 (Figs. 3B and C). Lung tissues
313 infected with LPS, BJ501, and C57MA14 presented with enhanced STING and GSK3β
314 signaling (Fig. 3D). H151 inhibited STING activation, NF-κB phosphorylation at
315 Ser536, IRF3 phosphorylation at Ser396, and IL-6 expression in LPS-infected lungs
316 (Fig. 3E). It also lowered serum IL-6 and protected the lungs against inflammatory
317 injury at 1 dpi (Figs. 3F and G). Thus, STING and GSK3β might play crucial roles in
318 the acute inflammatory response triggered by LPS, Poly(I:C), and SARS-CoV-2.

319 *3.4 The inhibition of TBK1 phosphorylation also attenuated IL-6 upregulation induced*
320 *by LPS, Poly(I:C), and SARS-CoV-2*

321 TBK1 is essential for activating NF-κB and releasing IL-6 downstream [22].
322 TBK1 phosphorylation at Ser172 was detected in lung tissues and cells infected with
323 LPS, Poly(I:C), or SARS-CoV-2 (Figs. 4A and B). After GSK8612 (TBK1 inhibitor)
324 suppressed TBK1 phosphorylation, IRF3 and NF-κB phosphorylation and IL-6
325 expression also decreased in RAW246.7 cells infected with LPS, Poly(I:C), or SARS-
326 CoV-2 (Fig. 4C). In vivo experiments disclosed that GSK8612 lowered serum IL-6
327 levels (Fig. S3A) and attenuated acute inflammatory lung injury in LPS- and H1N1-
328 infected mice (Fig. S3B). GSK8612 significantly inhibited LPS- and H1N10-induced
329 TBK1, IRF3, and NF-κB phosphorylation (Fig. S3C). Similarly, inosine suppressed
330 TBK1, IRF3, and NF-κB phosphorylation promoted by LPS, SARS-CoV-2, or Poly(I:C)
331 infection (Figs. 4D and E and Fig. S3D). The inhibition of TBK1 phosphorylation by
332 inosine drastically reduced the levels and nuclear translocation of phosphorylated IRF3

and NF-κB (Fig. 4F and Fig. S3E). However, inosine did not hinder binding between TBK1 and IRF3 in HEK-293 cells overexpressing the former (Fig. 4G). Therefore, TBK1 phosphorylation is strongly associated with the proinflammatory response and IL-6 upregulation promoted by the foregoing infectious agents and is a potential inosine target.

3.5 STING and GSK3β promoted TBK1 phosphorylation and IL-6 expression

To determine whether innate immune signaling is implicated in TBK1 phosphorylation and IL-6 upregulation, we inhibited STING or GSK3β in mononuclear macrophages infected with LPS, Poly(I:C), or SARS-CoV-2. H151 and TWS119 significantly inhibited LPS- and SARS-CoV-2-induced TBK1 phosphorylation as well as IL-6 expression in infected cells (Figs. 5A and B). TWS119 negated Poly(I:C)-induced increases in TBK1 phosphorylation and cytoplasmic IL-6 content (Fig. 5B). In vitro and in vivo experiments revealed that inosine inhibited STING and GSK3β phosphorylation induced by various infectious agents (Figs. 5C and D). $A_{2A}R$ mediates the anti-inflammatory action of inosine by downregulating IL-6. Nevertheless, the $A_{2A}R$ agonist regadenoson could not oppose IL-6 upregulation in infected RAW246.7 cells (Fig. 5E). STING, GSK3β, and TBK1 evoke acute inflammatory responses to LPS, Poly(I:C), or SARS-CoV-2 infection. The preceding results imply that inosine may target STING and GSK3β. As both of these are upstream TBK1 regulators, inosine indirectly suppresses TBK1 phosphorylation and IL-6 upregulation induced by multiple stimuli.

3.6 Inosine inhibited TBK1 phosphorylation by interfering with STING and GSK3β

activation

We performed a biotin pulldown assay and molecular docking to clarify the mechanism by which inosine inhibits TBK1 phosphorylation. First, we introduced long-chain biotin via esterification of the hydroxyl group to construct a biotinylated inosine (Fig. 6A). It was confirmed that the latter also had anti-inflammatory efficacy as it suppressed proinflammatory signals (STING or GSK3β) and TBK1-mediated IL-6 expression in LPS- and Poly(I:C)-infected cells (Figs. S4C and D). Next, our pulldown analysis with silver staining disclosed that, relative to biotin, Bio-inosine significantly enhanced protein precipitation at 33−35 kDa and 40−55 kDa. However, unlabeled inosine at tenfold the Bio-inosine concentration competitively reduced the precipitation of proteins targeted by Bio-inosine (Fig. 6B). Western blot demonstrated that the precipitated protein bands included STING and GSK3β (Fig. 6C). Hence, binding occurred directly between inosine and these proteins. Flag-tagged STING and GSK3β proteins were expressed in the HEK293 cells (Fig. S4E). Cell lysates were also tested in the biotin pulldown assays with and without Bio-inosine. The latter precipitated Flag-tagged STING and GSK3β. Tenfold excess unlabeled free inosine blocked binding between Bio-inosine and STING or GSK3β (Fig. 6D). We performing a docking analysis to clarify the mode of inosine binding to STING or GSK3β. Figures 6E and F show that inosine binds human STING in the pocket between the two chains along with the kinase binding domain of human GSK3β. Van der Waals and π-π stacking interactions formed between inosine and STING or GSK3β (Figs. 6E and F). The docking scores of inosine with human STING and GSK3β were −6.77 kcal/mol

and −8.16 kcal/mol, respectively. The foregoing discoveries suggest that inosine directly targets STING and GSK3β, inhibits their phosphorylation, and suppresses the TBK1-mediated proinflammatory response.

4. Discussion

Uncontrolled, hyperactivate inflammatory responses are believed to be the principal triggers of SARS-CoV-2-induced acute lung injury and are closely associated with COVID-19 severity and mortality. The present study identified inosine as a broad-spectrum anti-inflammatory that might effectively alleviate acute inflammatory lung injury induced by multiple infectious agents. Inosine substantially improved survival in SARS-CoV-2-infected mice mainly by suppressing the release of IL-6 and other proinflammatory cytokines. Inosine interacted with STING and GSK3β, inhibited their phosphorylation, significantly decreased TBK1 phosphorylation, suppressed the proinflammatory nuclear factors NF-κB and IRF3, and downregulated proinflammatory IL-6 in response to pathogen attack and invasion. This study demonstrated the critical role of TBK1 in acute inflammatory lung injury evoked by various infectious agents and indicated that inosine and other drugs targeting TBK1 are potential therapeutic strategies against COVID-19.

Megakaryocytes and monocytes synthesize and secrete the proinflammatory cytokines, which are major clinical features of COVID-19. These cells and substances promote disease progression via acute inflammatory lung injury [30, 31]. SARS-CoV-2 and other infectious agents indeed trigger severe pulmonary inflammatory responses including the pathological features of pneumonia and cytokine storms [32, 33].

Effective cytokine storm management could improve outcomes and survival in patients with COVID-19. Standard clinical anti-cytokine therapies include glucocorticoid and cytokine antagonist administration. In contrast, inosine suppresses but does not abolish the release of the proinflammatory cytokines IL-6 induced by SARS-CoV-2. Nevertheless, it also upregulates the anti-inflammatory cytokine IL-10. Hence, it could attenuate the cytokine response. For these reasons, inosine significantly improved survival in SARS-CoV-2-infected mice even without directly inhibiting viral replication. Inosine indistinguishably alleviated the lung tissue damage and lowered the serum levels of IL-6. This factor is thought to be a major component of the cytokine storm and is correlated with COVID-19 severity and mortality. In fact, inosine administration might prevent pulmonary injuries resulting from acute inflammation caused by multiple stimuli. Hence, inosine might deploy the same anti-cytokine storm mechanisms including IL-6 inhibition against SARS-CoV-2, other viruses, and bacterial pathogens.

Our study demonstrated that SARS-CoV-2 activated the NF-κB transcription factor (TF) that induces cytokine genes in response to viral or bacterial infection. Early in infection, phosphorylated NF-κB and its cascade co-activators induce IL-6 and TNF-α. Phosphorylation of the TF IRF3 was also detected in SARS-CoV-2-infected macrophages and lungs. After IRF3 senses viral RNA and cytoplastic DNA, it induces type I interferon (IFN) secretion [34, 35]. Nevertheless, neither the present nor previous studies detected any significant elevation in the type I IFN response in severe SARS-CoV-2 infection (Fig. S2B). By contrast, SARS-CoV-2 infection remarkably

upregulated serum IFN-γ at 3 dpi. Therefore, IRF3 activation might contribute to IFN-γ induction. A recent study reported that IL-6 is a non-canonical interferon-stimulated gene (ISG) responding to IFN signaling [36]. For this reason, IRF3 activation might be implicated in SARS-CoV-2-induced IL-6 expression. SARS-CoV-2-elicited cytokine release may be correlated with multiple cellular pathways or networks such as NF-κB and IRF3 signaling. LPS, Poly(I:C), and H1N1 induced NF-κB and IRF3 phosphorylation which, in turn, first upregulated IL-6 and TNF-α and then IFN-γ. In response to all infectious agents, inosine had excellent anti-cytokine efficacy as it suppressed the release of IL-6 mainly by inhibiting NF-κB and IRF3 phosphorylation.

Purinergic receptors are expressed by a wide range of immune cells and might have various anti-inflammatory effects [37]. $A_{2A}R$ mediates the anti-cytokine effects of inosine in LPS-induced acute lung injury [38, 39]. However, selective A_{2A} adenosine receptor agonists did not abrogate elevated inflammation associated with transcription signaling or IL-6 upregulation in response to multiple stimuli. Thus, the anti-inflammatory effects of inosine are not $A_{2A}R$-dependent. TBK1 is the gatekeeper of bacterial and viral-induced inflammatory signaling crossroads [22, 40] and was strongly phosphorylated in macrophages and lung tissues infected with LPS, Poly(I:C), H1N1, or SARS-CoV-2. TBK1 phosphorylation is essential for the recruitment and phosphorylation of the downstream TFs NF-κB and IFR3. TBK1 also promotes the nuclear translocation of phosphor-NF-κB and phosphor-IFR3 which, in turn, regulate proinflammatory cytokine expression [22]. The inhibiting of TBK1 phosphorylation via inosine or the administration of a selective TBK1 inhibitor significantly attenuated the

443 NF-κB and IRF3 responses and acute inflammatory pulmonary injury but allowed IL-
444 6 upregulation. In a TBK-1-dependent manner, inosine downregulated IL-6 and
445 improved the morphology and histology of lungs infected with SARS-CoV-2 and other
446 agents.

447 The results of our results demonstrated that inosine did not interfere with TBK1
448 phosphorylation via direct binding. Rather, it suppressed STING and GSK3β
449 phosphorylation. STING and GSK3β antagonists markedly reduced SARS-CoV-2- and
450 LPS-induced increases in TBK1 phosphorylation and IL-6 expression. STING is a
451 scaffold for the phosphorylation of TBK1 and itself [41]. Residues 1–341 formed
452 dimers or orchestrated oligomers to trigger STING and TNK1 phosphorylation. The
453 STING dimers had α-type loops in the cytosolic ligand-binding domain of STING and
454 participated in the formation of tetramer interfaces for cyclic GMP-AMPP (cGAMP)
455 binding. Cyclic GMP-AMPP is an endogenous secondary messenger of cGAS signaling
456 that participates in STING phosphorylation and interferon production [41, 42]. Inosine
457 made no contact with the *C*-terminal residues of STING which are the TBK1 binding
458 sites. However, inosine bound human STING residues in the pocket between the two
459 chains. One of these (Glu260) is adjacent to a tetramer interface site (Gln273) [41].
460 Inosine may inhibit the phosphorylation of STING by interfering with its dimerization
461 or its interaction with cGAMP. Our *in silico* docking and biotin pulldown assays
462 confirmed that inosine directly interacts with GSK3β, Val70, and Val 135. The latter
463 residues are implicated in GSK3β inhibition [43]. When viral infections are perceived,
464 ubiquitinated tripartite motif 9 short isoforms (TRIM9s) bridge activated GSK3β and

TBK1 [35] and the latter is then autophosphorylated. STING and GSK3β play critical roles in TBK1 phosphorylation while inosine indirectly suppresses TBK1 activation induced by SARS-CoV-2 and other infectious agents.

5. Conclusions

The present study empirically demonstrated that inosine administration improved survival in severe SARS-CoV-2 infection through its immunomodulatory but not immunosuppressive efficacy against acute inflammatory lung injury. As presented in Fig. 6G, inosine indirectly suppresses the phosphorylation of TBK1 at the crossroad of multiple innate immune responses. In this manner, it hinders overactivation of downstream cascade signaling and excessive proinflammatory cytokine release. Hence, inosine is potentially an excellent broad-spectrum anti-inflammatory agent. Future research should evaluate its clinical efficacy in the treatment of severe and critical COVID-19. Furthermore, TBK1 is a putative therapeutic target in the attenuation of cytokine storms and acute inflammatory lung injury induced by SARS-CoV-2 and other infectious agents.

CRediT author statement

Ningning Wang: Methodology, Investigation, Visualization and Writing-original draft; **Entao Li:** Methodology, Investigation and Writing-original draft; **Huifang Deng:** Methodology and Writing-original draft; **Lanxin Yue** and **Rina Su:** Investigation; **Lei Zhou** and **Baokun He:** Visualization; **Chengcai Lai** and **Gaofu Li:** Methodology; **Yuwei Gao:** Funding acquisition, Project administration, Supervision and Writing-

review & editing; **Wei Zhou:** Conceptualization**,** Visualization, Supervision, Writing-original draft and Writing-review & editing; **Yue Gao:** Conceptualization**,** Funding acquisition, Project administration, Supervision and Writing-review & editing

Declaration of competing interest

Yue Gao, **Wei Zhou**, **Yuwei Gao**, **Ningning Wang** and **Entao Li** report a pending China patent application (No. 202111541575.0). **Yue Gao**, **Wei Zhou**, **Yuwei Gao** and **Ningning Wang** are the inventors of a pending PTC patent application (No. PCT/CN2022/078715) entitled "Application of inosine in the treatment for COVID-19".

Acknowledgments

This work was supported by grants from the Young Elite Scientists Sponsorship Program by CAST (No. 2021-QNRC1-03) and the National Key research and Development Program of China (No. 2020YFC0845400). We thank Prof. Hui P. Chen for help advice to experiments.

500 **References**

501 [1] A. Martinez Mesa, E. Cabrera Cesar, E. Martin-Montanez, et al., Acute Lung Injury
502 Biomarkers in the Prediction of COVID-19 Severity: Total Thiol, Ferritin and
503 Lactate Dehydrogenase, Antioxidants (Basel Switzerland). 10 (2021) 1221.
504 [2] A.M. Edwards, R.S. Baric, E.O. Saphire, et al., Stopping pandemics before they
505 start: Lessons learned from SARS-CoV-2, Science. 375 (2022) 1133-1139.
506 [3] W. Zhou, Y. Liu, D. Tian, et al., Potential benefits of precise corticosteroids therapy
507 for severe 2019-nCoV pneumonia, Signal Transduct Target Ther. 5 (2020) 18.
508 [4] R. Dal-Re, S.L. Becker, E. Bottieau, et al., Availability of oral antivirals against
509 SARS-CoV-2 infection and the requirement for an ethical prescribing approach,
510 Lancet Infect Dis. 22 (2022) e231–e238.
511 [5] R. Karki, B.R. Sharma, S. Tuladhar, et al., Synergism of TNF-α and IFN-γ Triggers
512 Inflammatory Cell Death, Tissue Damage, and Mortality in SARS-CoV-2
513 Infection and Cytokine Shock Syndromes, Cell. 184 (2021) 149-168.e17.
514 [6] R.Q. Cron, R. Caricchio, W.W. Chatham, Calming the cytokine storm in COVID-
515 19, Nat Med. 27 (2021) 1674–1675.
516 [7] P.F. Dequin, N. Heming, F. Meziani, et al., Effect of Hydrocortisone on 21-Day
517 Mortality or Respiratory Support Among Critically Ill Patients With COVID-19:
518 A Randomized Clinical Trial, JAMA. 324 (2020) 1298–1306.
519 [8] B.M. Tomazini, I.S. Maia, A.B. Cavalcanti, et al., Effect of Dexamethasone on Days
520 Alive and Ventilator-Free in Patients With Moderate or Severe Acute Respiratory
521 Distress Syndrome and COVID-19: The CoDEX Randomized Clinical Trial,

JAMA. 324 (2020) 1307-1316.

[9] R. Huang, C. Zhu, W. Jian, et al., Corticosteroid therapy is associated with the delay of SARS-CoV-2 clearance in COVID-19 patients, Eur J Pharmacol. 889 (2020), 173556.

[10] D.C. Fajgenbaum, C.H. June, Cytokine Storm, New England Journal of Medicine. 383 (2020) 2255-2273.

[11] W. Zhou, Y. Liu, B. Xu, et al., Early identification of patients with severe COVID-19 at increased risk of in-hospital death: a multicenter case-control study in Wuhan, J Thorac Dis. 13 (2021) 1380-1395.

[12] L.Y.C. Chen, R.L. Hoiland, S. Stukas, et al., Confronting the controversy: interleukin-6 and the COVID-19 cytokine storm syndrome, European Respiratory Journal. 56 (2020), 2003006.

[13] O.J. McElvaney, G.F. Curley, S. Rose-John, et al., Interleukin-6: obstacles to targeting a complex cytokine in critical illness, Lancet Respir Med. 9 (2021) 643-654.

[14] S.A. Jones, C.A. Hunter, Is IL-6 a key cytokine target for therapy in COVID-19?, Nat Rev Immunol. 21 (2021) 337-339.

[15] Z. Zhou, X. Zhang, X. Lei, et al., Sensing of cytoplasmic chromatin by cGAS activates innate immune response in SARS-CoV-2 infection, Signal Transduct Target Ther. 6 (2021) 382.

[16] N. Sugimoto, H. Mitoma, T. Kim, et al., Helicase proteins DHX29 and RIG-I cosense cytosolic nucleic acids in the human airway system, Proceedings of the

National Academy of Sciences. 111 (2014) 7747-7752.

[17] Y. Yu, Y. Liu, W. An, et al., STING-mediated inflammation in Kupffer cells contributes to progression of nonalcoholic steatohepatitis, Journal of Clinical Investigation. 129 (2019) 546-555.

[18] A. Park, A. Iwasaki, Type I and Type III Interferons - Induction, Signaling, Evasion, and Application to Combat COVID-19, Cell Host Microbe. 27 (2020) 870-878.

[19] S. Khan, M.S. Shafiei, C. Longoria, et al., SARS-CoV-2 spike protein induces inflammation via TLR2-dependent activation of the NF-kappaB pathway, Elife. 10 (2021), 68563.

[20] A.K. Rana, S.N. Rahmatkar, A. Kumar, et al., Glycogen synthase kinase-3: A putative target to combat severe acute respiratory syndrome coronavirus 2 (SARS-CoV-2) pandemic, Cytokine Growth Factor Rev. 58 (2021) 92-101.

[21] A. Marineau, K.A. Khan, M.J. Servant, Roles of GSK-3 and β-Catenin in Antiviral Innate Immune Sensing of Nucleic Acids, Cells. 9 (2020) 897.

[22] S. Yum, M. Li, Y. Fang, et al., TBK1 recruitment to STING activates both IRF3 and NF-κB that mediate immune defense against tumors and viral infections, Proceedings of the National Academy of Sciences. 118 (2021), e2100225118.

[23] S. Srinivasan, A.G. Torres, L. Ribas de Pouplana, Inosine in Biology and Disease, Genes (Basel). 12 (2021) 600.

[24] L. Liaudet, J.G. Mabley, P. Pacher, et al., Inosine exerts a broad range of antiinflammatory effects in a murine model of acute lung injury, Ann Surg. 235 (2002) 568-578.

566 [25] L. Liaudet, J.G. Mabley, F.G. Soriano, et al., Inosine reduces systemic
567 inflammation and improves survival in septic shock induced by cecal ligation and
568 puncture, Am J Respir Crit Care Med. 164 (2001) 1213-1220.
569 [26] L.P. Chen, Y.M. Cai, J.S. Li, Medication rules of famous veteran traditional
570 Chinese medicine doctor in treatment of chronic bronchitis based on implicit
571 structure model, Zhongguo Zhong Yao Za Zhi. 42 (2017) 1609-1616.
572 [27] C. Ding, Z. Song, A. Shen, et al., Small molecules targeting the innate immune
573 cGAS–STING–TBK1 signaling pathway, Acta Pharm Sin B. 10 (2020) 2272-2298.
574 [28] Y. Liu, W. Liu, Z. Liang, Endophytic bacteria from Pinellia ternata, a new source
575 of purine alkaloids and bacterial manure, Pharm Biol. 53 (2015) 1545-1548.
576 [29] M. Ogasawara, K. Yoshii, J. Wada, et al., Identification of guanine, guanosine, and
577 inosine for α-amylase inhibitors in the extracts of the earthworm Eisenia fetida and
578 characterization of their inhibitory activities against porcine pancreatic α-amylase,
579 Enzyme Microb Technol. 142 (2020), 109693.
580 [30] L. Zhu, P. Yang, Y. Zhao, et al., Single-Cell Sequencing of Peripheral Mononuclear
581 Cells Reveals Distinct Immune Response Landscapes of COVID-19 and Influenza
582 Patients, Immunity. 53 (2020) 685-696 e683.
583 [31] X. Ren, W. Wen, X. Fan, et al., COVID-19 immune features revealed by a large-
584 scale single-cell transcriptome atlas, Cell. 184 (2021) 1895-1913.e19.
585 [32] N.G. Ravindra, M.M. Alfajaro, V. Gasque, et al., Single-cell longitudinal analysis
586 of SARS-CoV-2 infection in human airway epithelium identifies target cells,
587 alterations in gene expression, and cell state changes, PLoS Biol. 19 (2021),

588 e3001143.

589 [33] R.T. Huang, D. Wu, A. Meliton, et al., Experimental Lung Injury Reduces Krüppel-
590 like Factor 2 to Increase Endothelial Permeability via Regulation of RAPGEF3-
591 Rac1 Signaling, Am J Respir Crit Care Med. 195 (2017) 639-651.

592 [34] S. Liu, X. Cai, J. Wu, et al., Phosphorylation of innate immune adaptor proteins
593 MAVS, STING, and TRIF induces IRF3 activation, Science. 347 (2015), aaa2630.

594 [35] D.B. Stetson, R. Medzhitov, Recognition of cytosolic DNA activates an IRF3-
595 dependent innate immune response, Immunity. 24 (2006) 93-103.

596 [36] E.R. Sang, Y. Tian, L.C. Miller, et al., Epigenetic Evolution of ACE2 and IL-6
597 Genes: Non-Canonical Interferon-Stimulated Genes Correlate to COVID-19
598 Susceptibility in Vertebrates, Genes (Basel). 12 (2021) 154.

599 [37] F. Dos Anjos, J.L.B. Simoes, C.E. Assmann, et al., Potential Therapeutic Role of
600 Purinergic Receptors in Cardiovascular Disease Mediated by SARS-CoV-2, J
601 Immunol Res. 2020 (2020), 8632048.

602 [38] M. Lovaszi, Z.H. Nemeth, W.C. Gause, et al., Inosine monophosphate and inosine
603 differentially regulate endotoxemia and bacterial sepsis, The FASEB Journal. 35
604 (2021), e21935.

605 [39] G.R. Milne, T.M. Palmer, Anti-inflammatory and immunosuppressive effects of
606 the A2A adenosine receptor, The Scientific World Journal. 11 (2011) 320-339.

607 [40] Y. Qin, Q. Liu, S. Tian, et al., TRIM9 short isoform preferentially promotes DNA
608 and RNA virus-induced production of type I interferon by recruiting GSK3β to
609 TBK1, Cell Res. 26 (2016) 613-628.

610 [41] C. Zhang, G. Shang, X. Gui, et al., Structural basis of STING binding with and
611 phosphorylation by TBK1, Nature. 567 (2019) 394-398.
612 [42] D.L. Burdette, K.M. Monroe, K. Sotelo-Troha, et al., STING is a direct innate
613 immune sensor of cyclic di-GMP, Nature. 478 (2011) 515-518.
614 [43] D. Zhang, L. Liu, L. Pang, et al., Biological evaluation and energetic analyses of
615 novel GSK-3β inhibitors, J Cell Biochem. 119 (2018) 3510-3518.

Figure captions

Fig. 1. Inosine alleviated LPS- and H1N1 virus-induced acute inflammatory lung injury. (A) C57BL/6 mice were challenged with 5 mg/kg LPS and administered 300 mg/kg inosine for 24 h. Lung tissue sections were stained with hematoxylin-eosin and injury was examined (n = 6). Scale bar = 200 μm. (B) Mice were treated as described in (A). Serum cytokine and chemokine levels were measured (n = 6). (C) Mice were treated with LPS and/or inosine for 24 h. IL-6 expression levels in lung tissue were detected by western blot. (D) RAW264.7 cells were treated with LPS and inosine for 24 h. IL-6 expression in RAW264.7 cells were measured by western blot (n = *3*). (E) Mice were infected with BJ501 and treated with 900 mg/kg inosine for 24 h. Quantitative ELISA of serum IL-6 (n = 6). (F) Mice were treated as described in (E). Pathological damage to lung tissue was examined by H&E staining (n = 6). Scale bar = 200 μm. Ctrl: control group; LPS: LPS-induced acute lung injury and no other treatment; LPS + Inosine: LPS-induced acute lung injury followed by inosine treatment; LPS+DXM: LPS-induced acute lung injury followed by dexamethasone treatment as positive control; BJ501: H1N1-induced acute lung injury and no other treatment; BJ501+Inosine: BJ501-induced acute lung injury followed by inosine treatment; BJ501+DXM: BJ501-induced acute lung injury followed by dexamethasone treatment as positive control. Data are means ± SEM. $^{*}P < 0.05$, $^{**}P < 0.01$, $^{***}P < 0.001$, $^{****}P < 0.0001$ vs. control. $^{\#}P < 0.05$, $^{\#\#}P < 0.01$, $^{\#\#\#}P < 0.001$, $^{\#\#\#\#}P < 0.0001$ vs. LPS or BJ501 group.

Fig. 2. Inosine ameliorated SARS-CoV-2-induced acute lung injury. BALB/C mice were intranasally infected with 0.1*LD_{50} C57MA14 and administered oral inosine for

1 day, 3 days, or 14 days. (A) Schematic of C57MA14 infection and oral inosine administration started at 24 h before infection. Samples were harvested on indicated days after inosine treatment. (B) Viral RNA loads in lung tissue were detected by RT-qPCR and $TCID_{50}$. (C) Cytokines in mouse sera were quantified by mouse cytokine panel (n = 8−12). (D) Pathological damage to lung tissue was examined by H&E staining (n = 6). Scale bar = 200 μm. (E) Survival and (F) daily weight change in mice infected with C57MA14 and treated with inosine for 14 days (n = 20). (G) IL-6 expression in mouse lung tissue evaluated by western blot. (H) C57MA14 (MOI = 0.1) exposure 1 h before 500 μM inosine administration for 24 h. IL-6 expression in RAW264.7 cells measured by western blot (n = 3). Ctrl: control group; C57MA14: SARS-CoV-2-induced acute lung injury and no other treatment; C57MA14 + Inosine: SARS-CoV-2-induced acute lung injury followed by inosine treatment. $^{*}P < 0.05$, $^{**}P < 0.01$, $^{***}P < 0.001$, $^{****}P < 0.0001$ vs. control. $^{\#}P < 0.05$, $^{\#\#}P < 0.01$, $^{\#\#\#}P < 0.001$, $^{\#\#\#\#}P < 0.0001$ vs. C57MA14 group.

Fig. 3. Infection activated STING and GSK3β signaling. (A) After 10 ng/mL LPS, C57MA14 (MOI = 0.1), or 50 μg/mL Poly(I:C) infection for 24 h, RAW264.7 cells were collected and lysed with specified antibodies for western blot (n = 3). (B-C) RAW264.7 cells were subjected to LPS or Poly(I:C) and treated with 10 μM H151 or 10 μM TWS119 for 24 h. NF-κB and IRF3 phosphorylation levels were measured by immunoblot (n = 3). (D) Mice were challenged with 5 mg/kg LPS, 0.1*LD_{50} BJ501, or 0.1*LD_{50} C57MA14. Lung tissue sections were stained with anti-p-STING (red) and anti-p-GSK3β (green) antibodies. Nuclei were stained with DAPI (blue) (n = 5). Scale

bar = 100 μm. (E) Mice were stimulated with LPS and treated with 7 mg/kg H151 for 24 h. Lung tissue sections were subjected to immunofluorescence assay with anti-p-STING (red), anti-IL-6 (green), anti-p-IRF3 (green), and anti-p-NF-κB (red) antibodies. Nuclei were stained with DAPI (blue) (n = 5). Scale bar = 100 μm. (F) Mice were treated as described in (D). Serum IL-6 in serum was measured by ELISA (n = 5). (G) Mice were treated as described in (D). Lung tissue sections were subjected to H&E staining (n = 5). Scale bar = 200 μm. p-GSK3β: anti-phospho-GSK3β; p-STING: anti-phospho-STING; p-IRF3: anti-phospho-IRF3, p-NF-κB: anti-phospho-NF-κB. $^{*}P < 0.05$, $^{**}P < 0.01$ vs. control. $^{\#}P < 0.05$, $^{\#\#}P < 0.01$ vs. LPS group.

Fig. 4. Inosine inhibited TBK1-mediated IL-6 production. (A) Western blot was used to detect p-TBK1 expression in mouse lung tissues (n = 3). (B) RAW264.7 cells were stimulated with 10 ng/mL LPS, C57MA14 (MOI = 0.1), or 50 μg/mL Poly(I:C) for 24 h. p-TBK1 expression was measured by western blot (n = 3). (C) RAW264.7 cells were exposed to LPS, Poly(I:C), or C57MA14 and treated with 10 μM GSK8612 for 24 h. TBK1, NF-κB, and IRF3 phosphorylation levels were determined by immunoblot (n = 3). (D) RAW264.7 cells were challenged with LPS, C57MA14, or Poly(I:C) and treated with 500 μM inosine for 24 h. Immunoblots of p-TBK1, p-NF-κB, and p-IRF3 in RAW264.7 cells (n = 3). (E) Western blot was used to measure p-TBK1, p-IRF3, and p-NF-κB expression in mouse lung tissues (n = 3). (F) Confocal fluorescence images of RAW264.7 cells infected with LPS or Poly(I:C) and treated with 500 μM inosine for 24 h (n = 3). Scale bar = 20 μm. (G) HEK293 cells were transfected with plasmids encoding HA-tagged TBK1. Cell lysates were precipitated with anti-HA antibody.

682 Immunoprecipitate was detected by western blot using specified antibodies (*n* = 3). p-
683 TBK1: anti-phospho-TBK1; HA: a protein tag based on human influenza virus
684 hemagglutinin antigen.

685 **Fig. 5.** STING and GSK3β promoted TBK1 phosphorylation and IL-6 expression. (A)
686 RAW264.7 cells were infected with 10 ng/mL LPS or C57MA14 (MOI = 0.1) and
687 treated with 1 μM H151 for ≤ 24 h. Western blot was used to measure p-TBK1 and IL-
688 6 expression in cell lysates (*n* = 3). (B) RAW264.7 cells were stimulated with LPS,
689 C57MA14, or Poly(I:C) and treated with 10 μM TWS119 for 24 h. Representative
690 western blot of p-TBK1 and IL-6 in cells (*n* = 3). (C) RAW264.7 cells were subjected
691 to LPS or C57MA14 and treated with 500 μM inosine for 24 h. Total proteins were
692 isolated and p-STING and p-GSK3β levels were probed (*n* = 3). (D) Mice were
693 subjected to 5 mg/kg LPS or 0.1*LD_{50} C57MA14 infection and administered inosine
694 for 24 h. Lung tissue sections were analyzed by immunofluorescent p-STING (red) and
695 p-GSK3β (green) co-staining. Nuclei were stained with DAPI (blue) (*n* = 5). Scale bar
696 = 100 μm. (E) RAW264.7 cells were infected with LPS, C57MA14, or Poly(I:C),
697 treated with regadenoson for 24 h, and subjected to western blot using indicated
698 antibodies (*n* = 3).

699 **Fig. 6.** Inosine directly targeted STING and GSK3β. (A) Synthesis and structure of
700 biotinylated inosine (Bio-inosine). (B-C) Bio-inosine or biotin was added to
701 streptavidin-agarose beads and incubated. Lysates prepared from RAW264.7 were
702 added to the streptavidin-agarose beads with Bio-inosine or biotin. Precipitates were
703 resolved by SDS-PAGE. Gel was stained with silver (B) and proteins were detected by

704 western blot as indicated (C). (D) STING and GSK3β plasmids were transfected into
705 HEK293 cells. After 24 h transfection, pulldown was performed using streptavidin-
706 agarose beads and subjected to western blot. (E) Schematic diagram of binding between
707 inosine and STING protein. Inosine binds STING in pocket between two chains.
708 Protein is shown in gray cartoon. Ligand is represented by cyan stick. (F) Schematic
709 diagram of binding between inosine and GSK3β protein. Inosine combined with
710 GSK3β kinase binding domain. Protein is shown in gray cartoon. Ligand is represented
711 by cyan stick. (G) Schematic diagram of mechanism by which inosine regulates
712 cytokine release.

713 **Fig. 1**

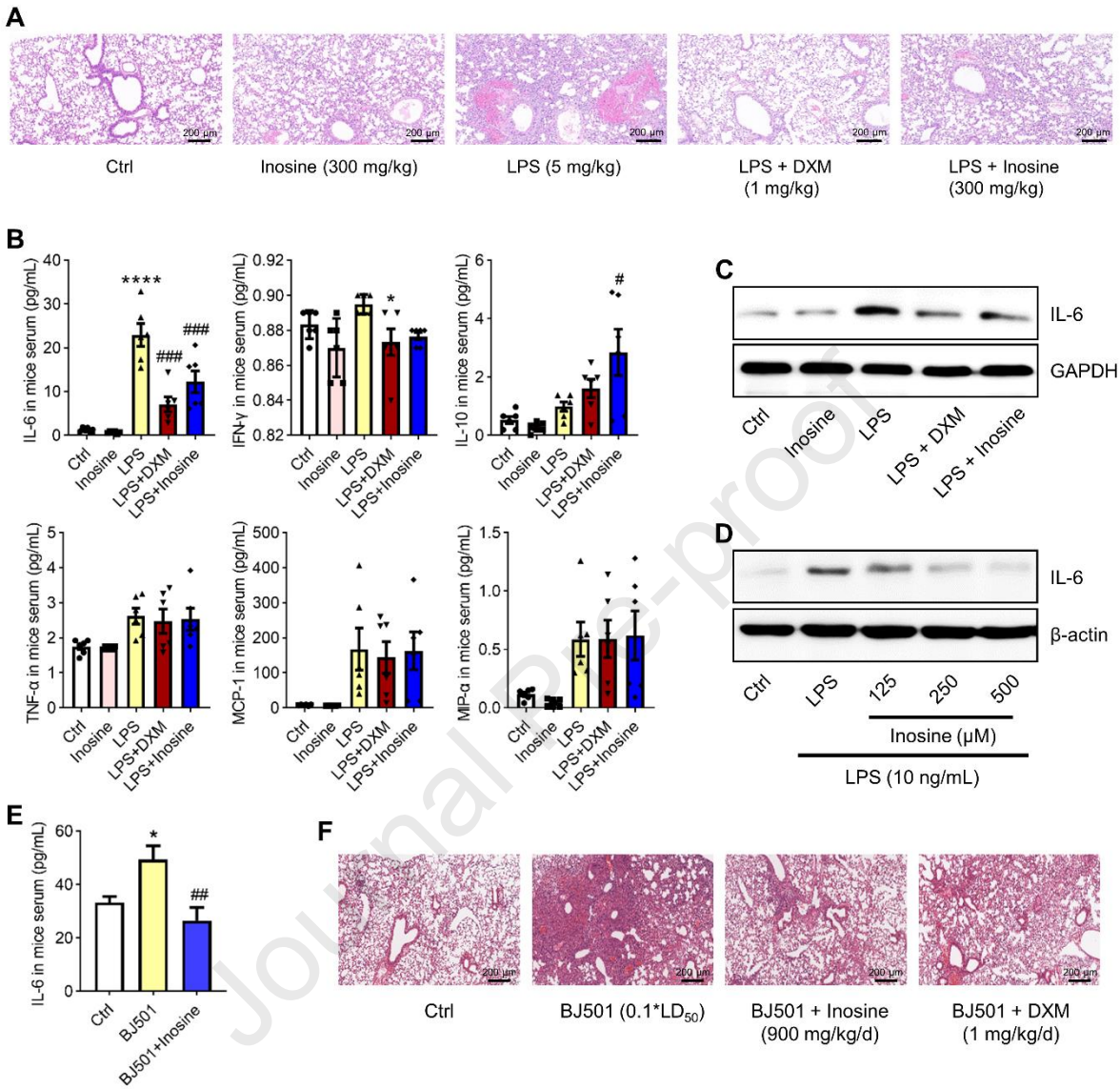

714

715 **Fig. 2**

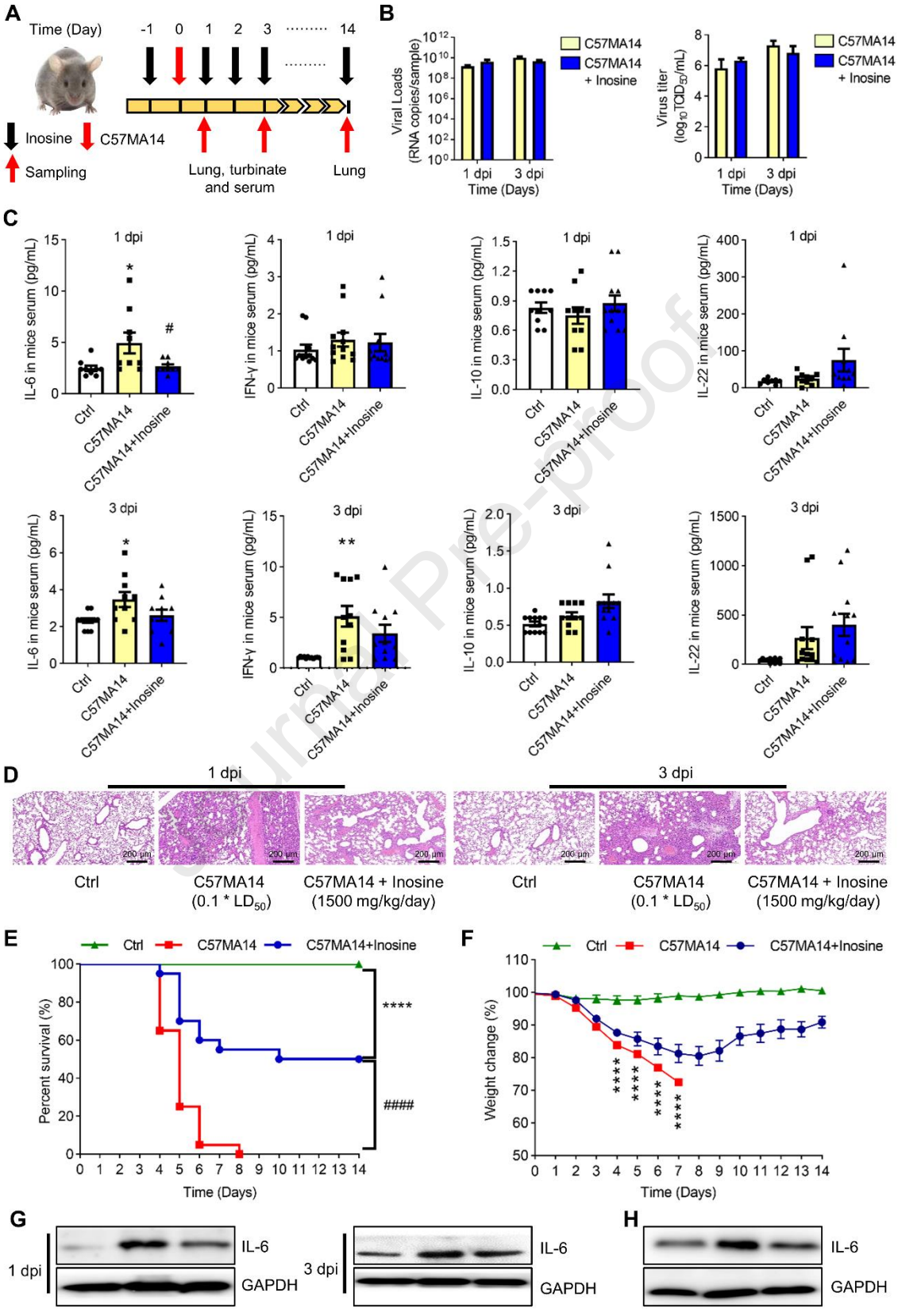
A
Time (Day)
-1 0 1 2 3 ····· 14
Inosine
C57MA14
Sampling
Lung, turbinate and serum
Lung
B
Viral Loads (RNA copies/sample)
C57MA14
C57MA14 + Inosine
1 dpi 3 dpi
Time (Days)
Virus titer ($log_{10}TCID_{50}$/mL)
C57MA14
C57MA14 + Inosine
1 dpi 3 dpi
Time (Days)
C
IL-6 in mice serum (pg/mL)
IFN-γ in mice serum (pg/mL)
IL-10 in mice serum (pg/mL)
IL-22 in mice serum (pg/mL)
1 dpi
3 dpi
Ctrl
C57MA14
C57MA14+Inosine
D
1 dpi
3 dpi
200 μm
Ctrl
C57MA14 (0.1 * LD_{50})
C57MA14 + Inosine (1500 mg/kg/day)
E
Ctrl
C57MA14
C57MA14+Inosine
Percent survival (%)
****
####
Time (Days)
F
Ctrl
C57MA14
C57MA14+Inosine
Weight change (%)
****
Time (Days)
G
1 dpi
3 dpi
IL-6
GAPDH
H
IL-6
GAPDH

716

717 **Fig. 3**

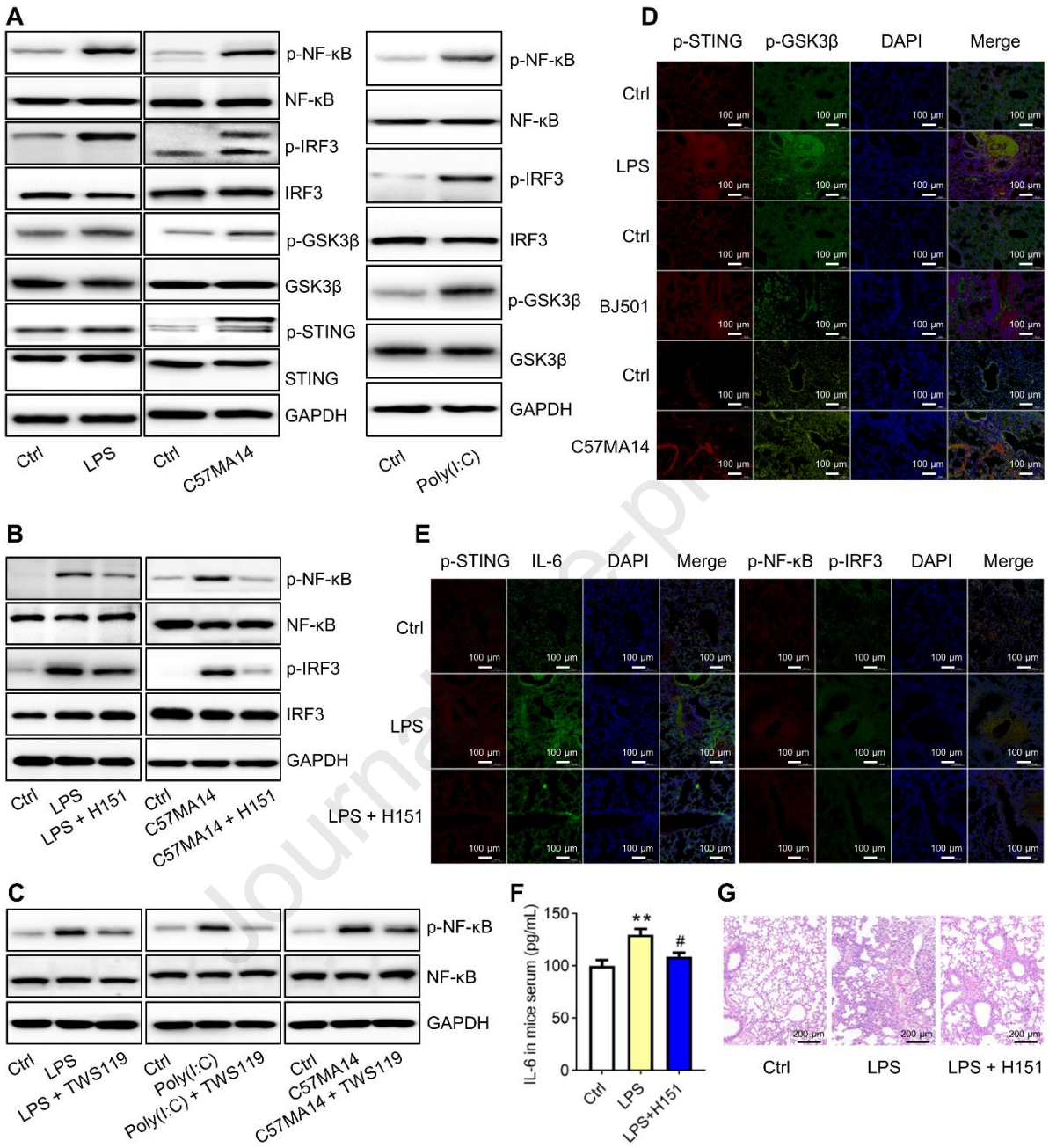
A
p-NF-κB
NF-κB
p-IRF3
IRF3
p-GSK3β
GSK3β
p-STING
STING
GAPDH
Ctrl
LPS
Ctrl
C57MA14
Ctrl
Poly(I:C)
D
p-STING
p-GSK3β
DAPI
Merge
Ctrl
LPS
Ctrl
BJ501
Ctrl
C57MA14
100 μm
B
p-NF-κB
NF-κB
p-IRF3
IRF3
GAPDH
Ctrl
LPS
LPS + H151
Ctrl
C57MA14
C57MA14 + H151
E
p-STING
IL-6
DAPI
Merge
p-NF-κB
p-IRF3
DAPI
Merge
Ctrl
LPS
LPS + H151
C
p-NF-κB
NF-κB
GAPDH
Ctrl
LPS
LPS + TWS119
Ctrl
Poly(I:C)
Poly(I:C) + TWS119
Ctrl
C57MA14
C57MA14 + TWS119
F
IL-6 in mice serum (pg/mL)
150
100
50
0
**
#
Ctrl
LPS
LPS+H151
G
200 μm
Ctrl
LPS
LPS + H151

718

719 **Fig. 4**

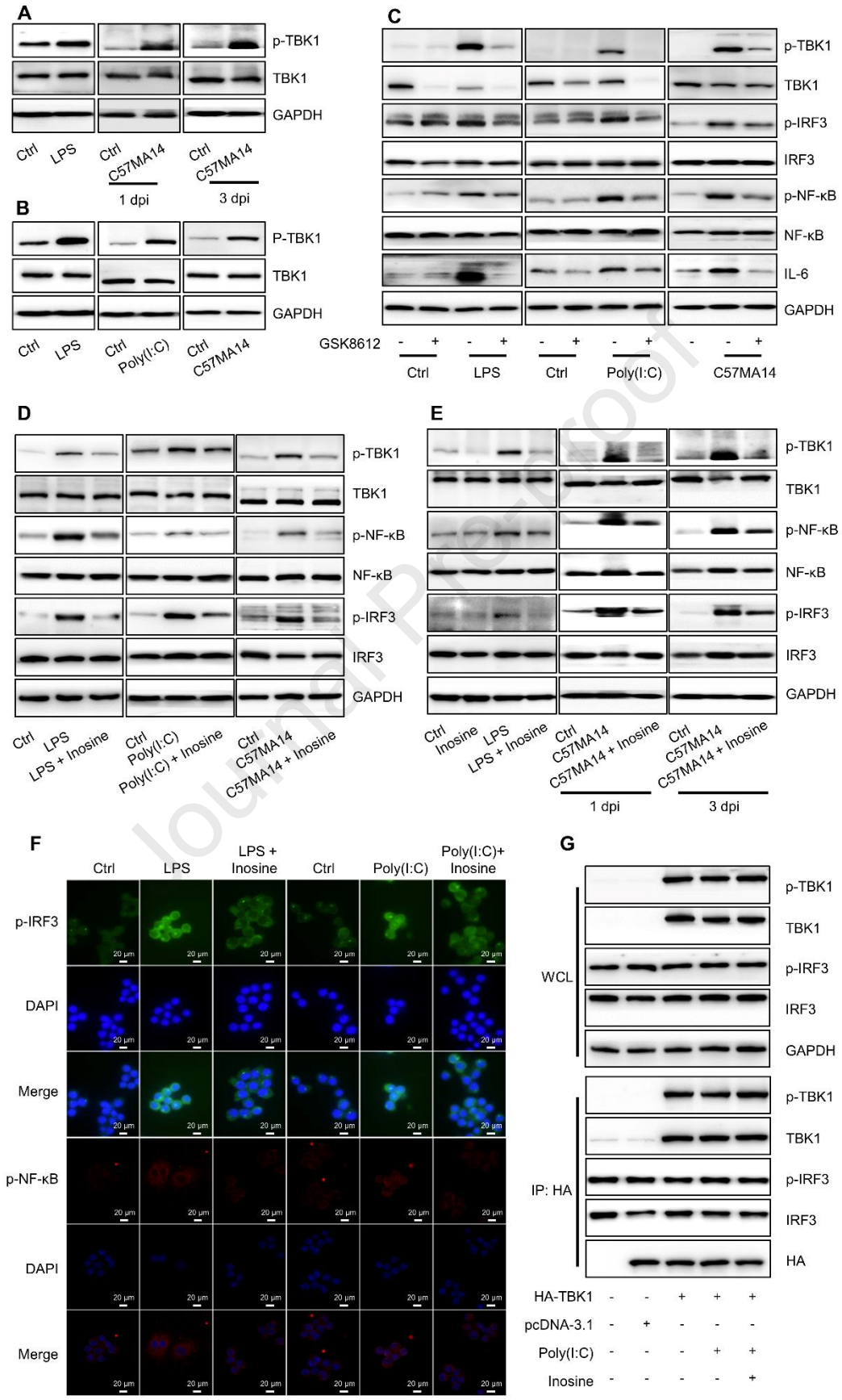
A
p-TBK1
TBK1
GAPDH
Ctrl
LPS
Ctrl
C57MA14
Ctrl
C57MA14
1 dpi
3 dpi
B
P-TBK1
TBK1
GAPDH
Ctrl
LPS
Ctrl
Poly(I:C)
Ctrl
C57MA14
C
p-TBK1
TBK1
p-IRF3
IRF3
p-NF-κB
NF-κB
IL-6
GAPDH
GSK8612
Ctrl
LPS
Ctrl
Poly(I:C)
C57MA14
D
p-TBK1
TBK1
p-NF-κB
NF-κB
p-IRF3
IRF3
GAPDH
Ctrl
LPS
LPS + Inosine
Ctrl
Poly(I:C)
Poly(I:C) + Inosine
Ctrl
C57MA14
C57MA14 + Inosine
E
p-TBK1
TBK1
p-NF-κB
NF-κB
p-IRF3
IRF3
GAPDH
Ctrl
Inosine
LPS
LPS + Inosine
Ctrl
C57MA14
C57MA14 + Inosine
Ctrl
C57MA14
C57MA14 + Inosine
1 dpi
3 dpi
F
Ctrl
LPS
LPS + Inosine
Ctrl
Poly(I:C)
Poly(I:C)+ Inosine
p-IRF3
DAPI
Merge
p-NF-κB
DAPI
Merge
20 μm
G
WCL
p-TBK1
TBK1
p-IRF3
IRF3
GAPDH
IP: HA
p-TBK1
TBK1
p-IRF3
IRF3
HA
HA-TBK1
pcDNA-3.1
Poly(I:C)
Inosine

720

721 **Fig. 5**

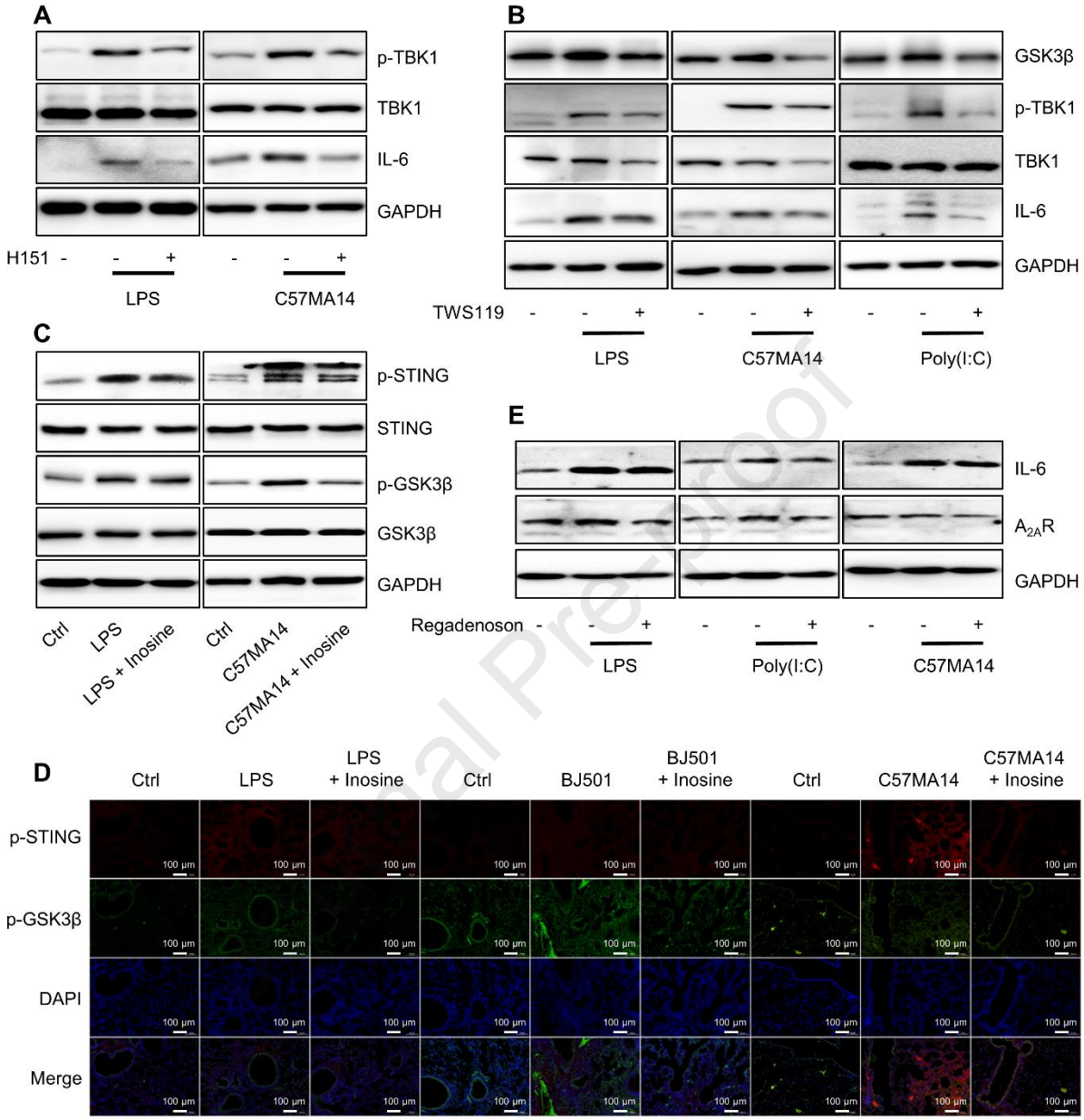
A
p-TBK1
TBK1
IL-6
GAPDH
H151 - - +
LPS
C57MA14
B
GSK3β
p-TBK1
TBK1
IL-6
GAPDH
TWS119 - - + - - + - - +
LPS
C57MA14
Poly(I:C)
C
p-STING
STING
p-GSK3β
GSK3β
GAPDH
Ctrl
LPS
LPS + Inosine
Ctrl
C57MA14
C57MA14 + Inosine
E
IL-6
A2AR
GAPDH
Regadenoson - - + - - + - - +
LPS
Poly(I:C)
C57MA14
D
Ctrl
LPS
LPS + Inosine
Ctrl
BJ501
BJ501 + Inosine
Ctrl
C57MA14
C57MA14 + Inosine
p-STING
p-GSK3β
DAPI
Merge
100 μm

722

723 **Fig. 6**

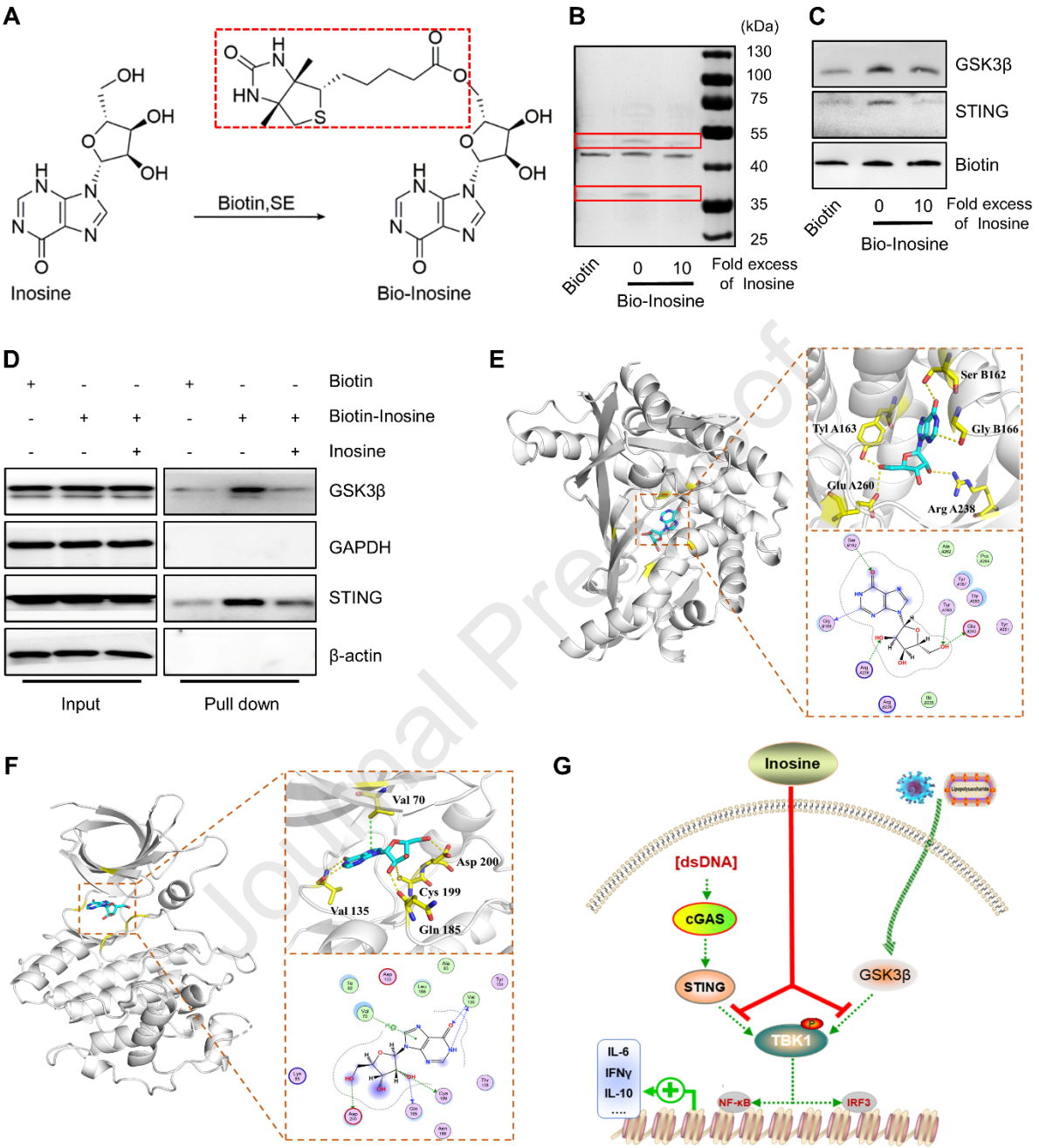

724

725

1. Inosine significantly improved the survival rate of SARS-CoV-2-infected mice.

2. Inosine obviously abrogated evoked excessive IL-6 expression but elevated IL-10 content, and eventually ameliorated acute inflammatory lung injury caused by multiple infectious agents.

3. Inosine indirectly interfered with the phosphorylation of TBK1 via binding to STING and GSK3β, leading to remarkable decreases in IL-6 release in serum and lung tissue of mice infected with LPS, H1N1 or SARS-CoV-2.